Technical design of the Phase I

Mu3e Experiment

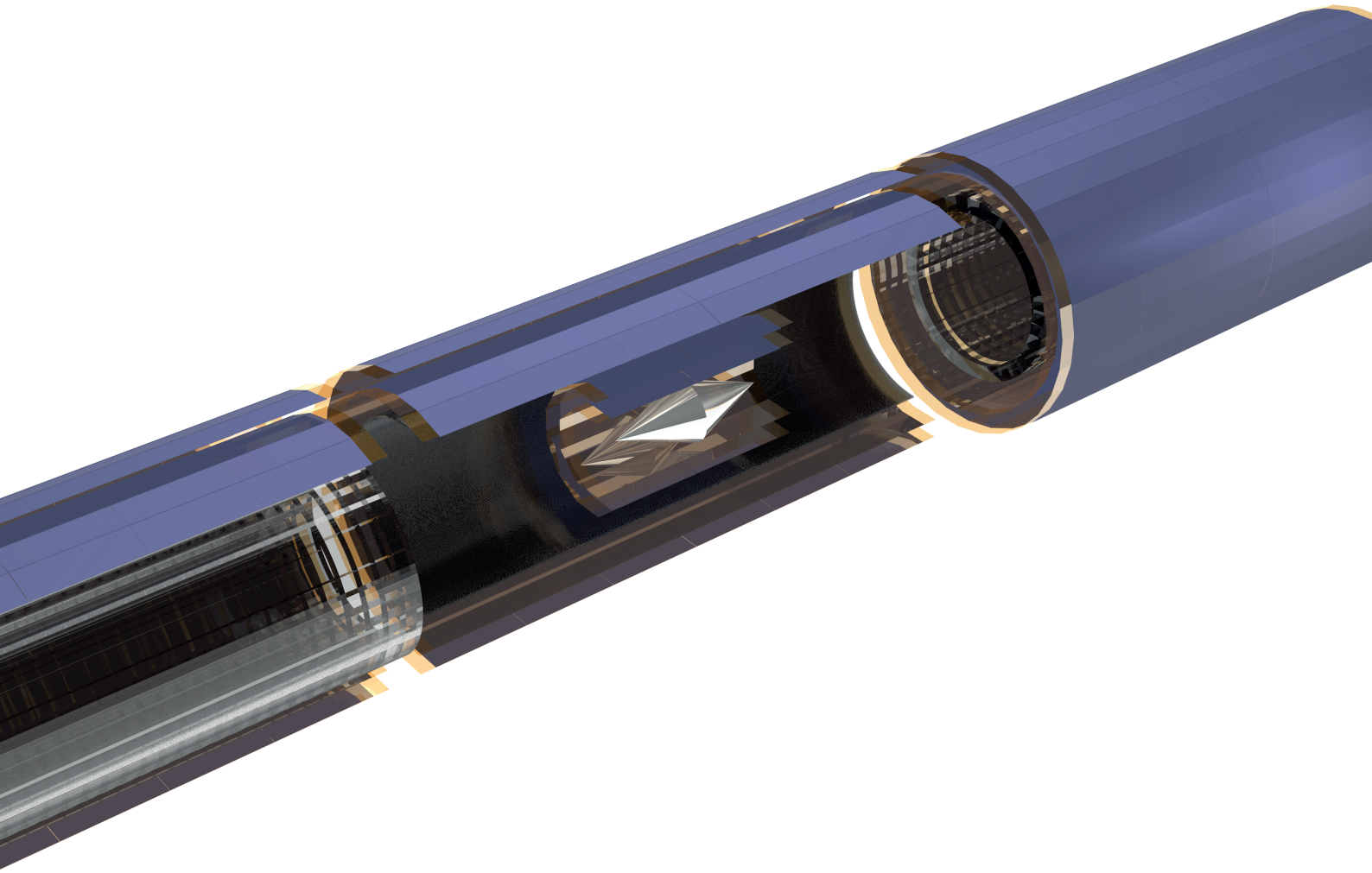

Chapter 1

Fiber Detector

To suppress all forms of combinatorial background, a very thin detector with good spatial and very good timing resolution, very high efficiency, and high rate capability is required in the central region of the Mu3e apparatus. To this aim, a thin Scintillating Fiber (SciFi) detector with few 100 ps time resolution, efficiency in excess of 96%, spatial resolution around 100 μm, and thickness $< 0.2\%$ of radiation length has been developed. Figure 1.1 shows the SciFi detector inside the Mu3e apparatus. In particular, the space constraints in the central part of the Mu3e apparatus impose a very compact design of the SciFi detector. Moreover the SciFi detector will help resolve the sense of rotation (i.e. the charge) of the recurling tracks in the central region of the apparatus.

The SciFi detector is cylindrical in shape, with a radius of about 6 cm and a length of 300 mm (280 mm in the acceptance / active part). It is composed of 12 SciFi ribbons 300 mm long and

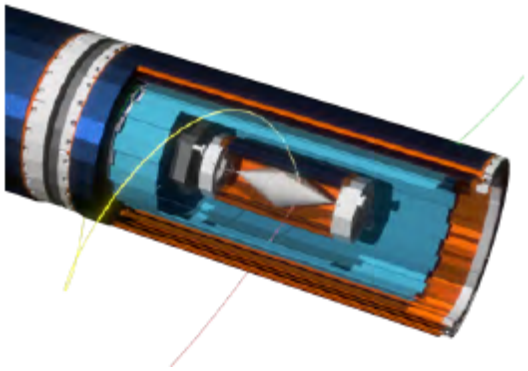

Figure 1.1: Open view of the central part of the Mu3e apparatus. The SciFi arrays are in blue.

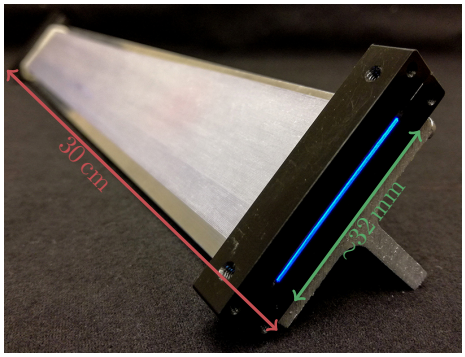

Figure 1.2: Full SciFi ribbon prototype with preliminary holding structure.

32.5 mm wide. The width of the ribbons matches the size of the photo-detector (see later). The detector is located just below the outer double-layer silicon pixel detector. During the last two years the design of the fiber detector has significantly evolved. In particular, the width of the SciFi ribbons has been increased from 16 mm to 32.5 mm, reducing thus the number of fiber ribbons by two and the length decreased from 360 mm to 300 mm, while the radius of the detector did not change. This reduces the number of components, simplifies the construction of the detector, and finally the installation.

We selected the 250 μm diameter multiclad round fibers from Kuraray, type SCSF-78MJ. Three SciFi layers are staggered in order to assure continuous coverage and high detection efficiency. Figure 1.2 shows a SciFi prototype, 32 mm wide and 300 mm long close to the final Mu3e design.

The SciFi arrays are coupled at both ends to silicon photomultiplier (SiPM) arrays. After careful evaluations we selected the 128 ch. LHCb Si-PM array from Hamamatsu, device S13552-HQR and are read out with a dedicated mixed mode ASIC, the MuTRiG.

By far the largest source of background to the $\mu^+ \to e^+e^-e^+$ search comes from the accidental combination of positron tracks from muon decays, in which two muons decay very close in space such that the decay vertices cannot be resolved. Moreover, if a decay positron undergoes Bhabha scattering it will eject one electron from the target, simulating the topology of a three prong muon decay. Such backgrounds can be efficiently suppressed by timing. Figure 1.3 shows the background suppression depending on the detector time resolution. Exploiting only the fibre detector, with a time resolution of 250 ps and a 90% overall efficiency, provides a survival fraction of background due to Bhabha electron/positron-pairs plus one Michel positron of $\mathcal{O}(3 \cdot 10^{-2})$, combining the fibre and tile detectors yields $\mathcal{O}(1.4 \cdot 10^{-2})$. [1]. For this study, we simulate a Bhabha electron-positron pair and a Michel positron from the same vertex, but distributed in a 50 ns time window for a beam intensity of 10^8 stopping μ^+ per second (Phase I). The three tracks are required to pass the kinematic signal selection cuts described in chapter **??**. By combining both detector systems, backgrounds can be reduced below the aimed sensitivity of 2×10^{-15} as illustrated in Figure 1.4. As can be noticed in Figure 1.4, the vertexing alone is not sufficient to suppress the background. The timing information from the SciFi detector with a conservative time resolution of 500 ps suppresses this background by almost 2 orders of magnitude in the signal region (down to a 10^{-18} level) making this measurement feasible.

[1] at a 90 % signal efficiency working point.

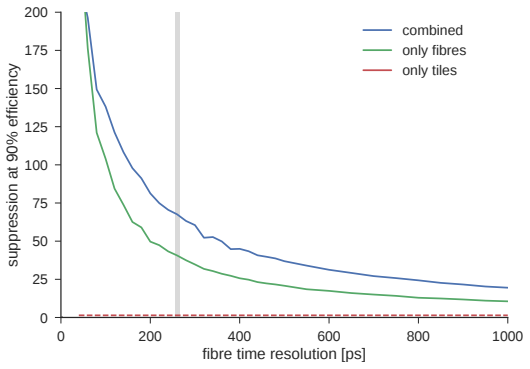

Figure 1.3: Suppression of Bhabha pair plus Michel accidental background as a function of fibre detector time resolution if both timing detectors (blue) are used or only the fibre detector (green) is used. A tile detector with a time resolution of 60 ps is assumed and a working point with a signal efficiency of 90 % for the combined suppression is chosen. The expected time resolution of the fibre detector is indicated in gray.

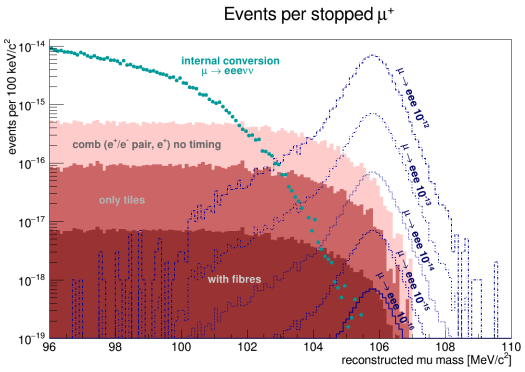

Figure 1.4: Reduction of the combinatorial background using the timing information. The SciFi timing information reduces this background by almost two orders of magnitude. Also shown is the irreducible background from muon radiative decays.

Figure 1.5 shows the time of flight of reconstructed track candidates between two consecutive SciFi detector crossings for recurling tracks. The time of flight in relation with the reconstructed trajectory's length allows one to reject misreconstructed track candidates with either wrong charge assignment or confused particle turns of recurling particles.

The fibre detector consists of the scintillating fibre ribbons as the active part, silicon photomultiplier (SiPM) arrays for light detection, a readout ASIC (the MuTRiG chip), further readout electronics and the support mechanics and cooling. These elements will be discussed in the following sections.

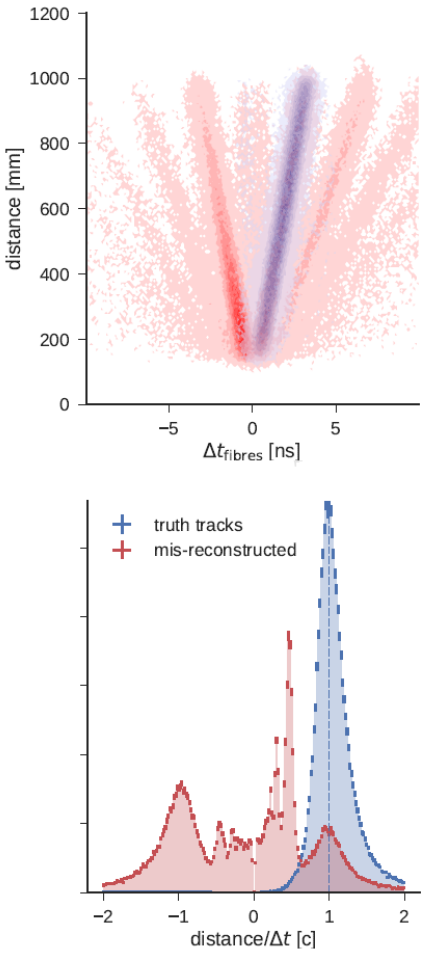

Figure 1.5: Rejection of mis-reconstructed track candidates by multiple fibre detector hits. Correct (blue) and mis-reconstructed (red) 8-hit track candidates with at least two hits in the fibre detector are shown. (top) Correlation between the length of the trajectory of a track candidate between the two fibre hits and the time difference between them. The different branches correspond to the combination of different segments of recurling tracks. (bottom) Corresponding velocity v = distance/Δt in terms of speed of light c of the track candidates. The different branches in the top plot correspond to the peaks in the bottom spectrum. Track candidates with $\Delta t < 0$, respectively $v < 0$, have a wrong charge assignment; hence the wrong rotation direction.

1.1 Fibre Ribbons

The surrounding pixel detector sets the dimensions of the fibre detector. The minimal active length of 280 mm is dictated by the acceptance of the pixel detector for tracks originating from the target. The SciFi detector is located in the central barrel right below the third pixel-based tracking layer at a radius of 61 mm. This particular value is set by the size of the photo-detector. The detector is segmented azimuthally into 12 SciFi ribbons each with a width of 32.5 mm, matching the size of the photo-detector. Each ribbon consists of three layers of 250 μm staggered SciFi (128 fibres per layer) with a length of 300 mm. Figures 1.2 and 1.6 show a fibre ribbon prototype with dimensions very close to final ribbons in the experiment.

Figure 1.6: Front view of a SciFi ribbon prototype with 120×3 fibres.

1.1.1 Fibres

The constraints on material budget, and also occupancy and position resolution, allow only for the thinnest available scintillating fibres (250 μm) to be used. In extensive measurement campaigns, we have performed a detailed comparison of different types of 250 µm round fibres produced by Kuraray (SCSF-78, SCSF-81, and NOL-11) and Saint-Gobain (BCF-12) and square cross-section fibres by Saint-Gobain (BCF-12). Table 1.1 summarizes the characteristics of different SciFi types.

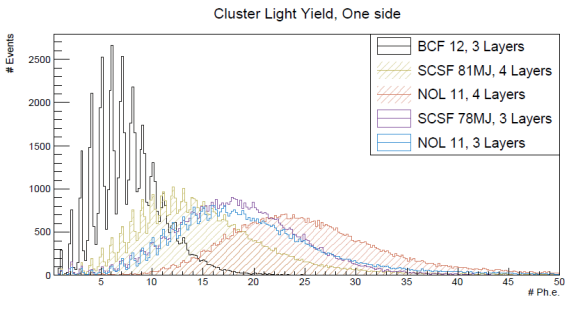

Figure 1.7: Light yield of different SciFi ribbons using different scintillating materials. The number of photoelectrons is the charge sum of all channels in a cluster at one side matched to a track. The minimal cluster multiplicity is two neighbouring channels with an amplitude of at least 0.5 ph.e. The histograms are normalised by their integral.

company	Saint-Gobain	Kuraray		R&D
type	BCF-12	SCSF-81MJ	SCSF-78MJ	NOL-11
emission peak [nm]	435	437	450	
decay time [ns]	3.2	2.4	2.8	1.1
attenuation length [m]	>2.7	>3.5	>4.0	
light yield [ph/MeV]	∼8000		high	high
refractive index	1.60/1.49/1.42	1.59/1.49/1.42		
density [g/cm^3]	1.05	1.05/1.19/1.43		
available shapes	round & square	round		round
cladding [%] round	3/1	3/3		
square	4/2	-	-	-
trapping [%] round	≥5.6	5.4		
square	7.3	-	-	-
core		Polystyrene (PS)		
inner cladding		Acrylic (PMMA)		
outer cladding		Fluor-acrylic (FP)		

Table 1.1: Properties of different scintillating fibre types from Kuraray and Saint Gobain [1,2]. NOL-11 is an R&D fibre with Kuraray involvement. Its properties are assumed to be very similar to the other Kuraray fibres. Light yield is only quoted by Saint-Gobain, whereas Kuraray characterises SCSF-78 and NOL-11 as "high light yield" fibres.

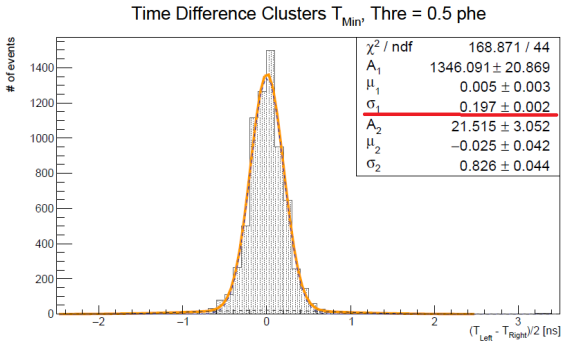

Figure 1.8: Time resolution (mean time) obtained with a 4 layer SciFi ribbon using Kuraray NOL-11 fibers.

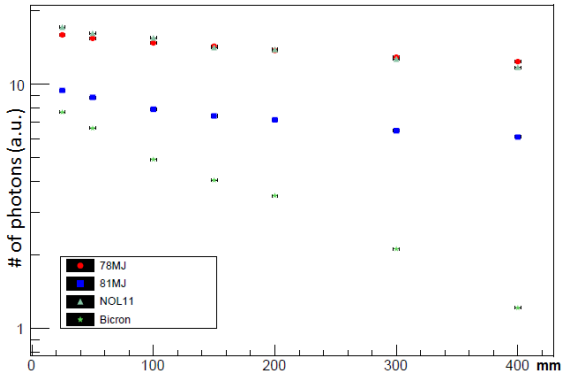

Figure 1.9: Light attenuation in different fiber types as a distance of the source.

Figure 1.7 shows the light yield for a m.i.p. crossing the SciFi ribbon for different fiber materials. The light yield is measured with respect to the center of the fiber ribbon (150 mm from the edge). As can be noticed the Kuraray SCSF-78 and NOL-11 fibers provide the highest light yields. Figure 1.8 shows the time performance obtained with the NOL-11 fiber; the achieved resolution on the mean time (i.e. using the timing measurements from both fiber ends) is around 200 ps (see later). Figure 1.9 compares the light yield as a function of the distance from the source (attenuation) of different fibers under the same conditions, so that the light yields from different fibers, even if not absolutely normalized, can be compared. The Kuraray fiber types SCSF-78 and NOL-11 are similar with the least attenuation and similar light yields, while surprisingly the BCF-12 fibers have a rather short attenuation length. More detailed results can be found in [3–5].

Based on their performance with respect to light yield and time resolution, as well as availability, round double-clad SCSF-78MJ fibres from Kuraray were chosen. Novel NOL fibres, based

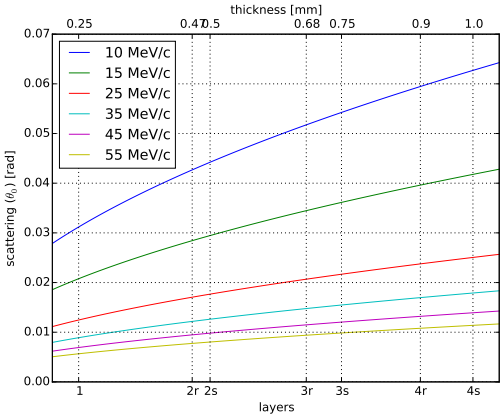

Figure 1.10: Multiple Scattering θ_0 depending on electron/positron momentum and fibre ribbon thickness. r indicates the thickness of round and s of square fibres.

on Nanostructured Organosilicon Luminophores, give the best performance, but will only become commercially available in the next years. Hence, they are a viable option for potential SciFi detector upgrades in the future.

1.1.2 Number of Layers

A critical point of optimization is the number of fibre layers. More layers lead to a better timing resolution and a higher efficiency but deteriorate the momentum resolution of the tracker due to multiple Coulomb scattering. In addition, more layers lead to larger cluster size and larger occupancy, which makes it harder to associate tracks and clusters of fibre hits.

Using the measured performance characteristics of the fibres, we have performed extensive simulation studies of the fibre detector resolution, efficiency and the effects on the track reconstruction and linking. Details on the complete detector simulation can be found in chapter **??**, the reconstruction algorithm is described in chapter **??** and the selection used to determine the performance on signal decays is detailed in chapter **??**.

The amount of multiple scattering caused by the fibres and the glue in the ribbons is shown in figure 1.10. Note that a ribbon of three layers of round 250 µm fibres corresponds to below 0.3 % X/X_0. This scattering affects the momentum resolution (see figure 1.11) and thus the

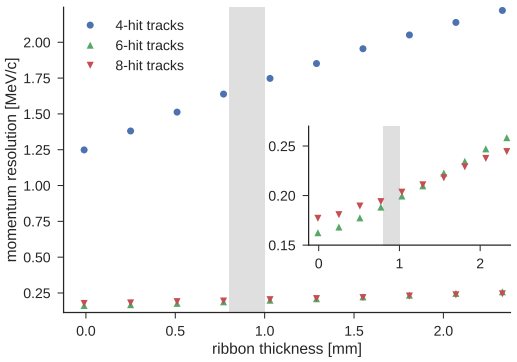

Figure 1.11: Momentum resolution for short (outgoing) and long (outgoing and recurling) tracks as a function of fibre ribbon thickness using simulated Michel decays. The targeted fibre ribbon thickness of ∼0.9 mm is highlighted. The momentum resolution of long (6- and 8-hit) tracks is improved over short (4-hit) tracks due to their recurling. The effect of the fibre detector is more pronounced for 6-hit than 8-hit tracks.

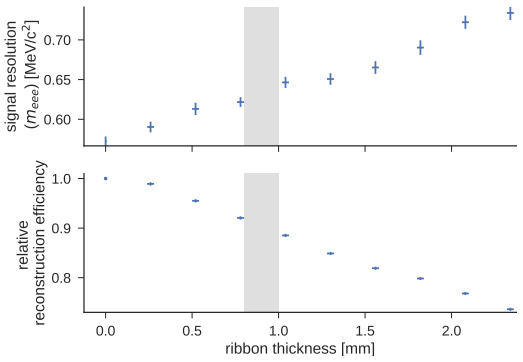

Figure 1.12: Signal resolution in terms of invariant mass of the three tracks of a candidate m_{eee} (top) and the relative reconstruction efficiency with respect to the absence of the fibre detector as a function of the fibre ribbon thickness. The planned ribbon thickness ∼0.9 mm is highlighted.

$\mu^+ \to e^+e^-e^+$ signal invariant mass resolution and reconstruction efficiency.

More fibre layers also lead to larger pile-up, i.e. hits from different tracks (or different turns of the same track) producing hits in the same fibre or in the same cluster of fibres and larger clusters.

As a compromise between the aforementioned constraints, three layers of 250 µm thick round

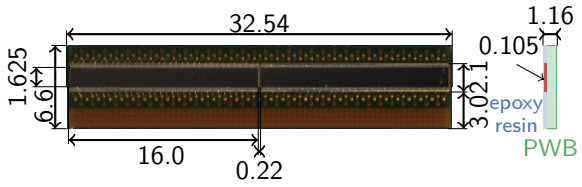

Figure 1.13: Picture of a Hamamatsu S13552-HRQ SiPM column array (left) and a schematic side view (right). All dimensions are given in units of mm. 24 such sensors are used in the Mu3e fibre detector.

characteristic	value
breakdown	51.0 V
variation per sensor	±250 mV
variation between sensors	±500 mV
temperature coefficient	53.7 mV/K
gain	$3.8 \cdot 10^6$
direct crosstalk	3 %
delayed crosstalk	2.5 %
after-pulse	0 %
peak PDE	48 %
max PDE wavelength	450 nm
mean quench resistance R_Q	490 kΩ at 25 °C
recovery time τ_{recovery}	68.9(21) ns
short component τ_{short}	< 1 ns
long component τ_{long}	50.1(41) ns

Table 1.2: SiPM (S13552-HRQ) characteristics at $\Delta T = 3.5$ V and $T = 25$ °C from [6].

fibres are chosen. With a thinner detector, it would be challenging to fulfill the efficiency requirements and the time resolution would not be sufficient for a reliable charge identification, e.g. rejection of mis-reconstructed track candidates.

1.2 Silicon Photomultiplier Arrays

The space constraints between the pixel detector layers and the strong magnetic field require the use of solid state photon detectors; in fact, the space constraints are so tight that silicon photomultiplier (SiPM) arrays are the only option. The compact form factors and moderate high voltage (∼ 60 V) of SiPM arrays account for the limited space and they provide the required channel density. They are insensitive to magnetic fields. The photon detection efficiency (PDE[2]) up to 50 %, single photon detection and very fast intrinsic time response (single photon jitter of approximately 200 ps) are the key features for the use in the fibre detector. The high gain (∼ 10^6) allows the use of mixed-mode ASICs (like MuTRiG) without any pre-amplification. Typical dark-rates of SiPMs are around a few 10 kHz per channel at room temperature, depending on the SiPM type.

The photons produced in the scintillating fibres are detected on both fibre ends in SiPM arrays. Acquiring the signals on both sides increases the time resolution, helps to distinguish between noise and signal and increases the detection efficiency of the whole system. Moreover, by taking the mean time of the two time measurements, the timing measurements is independent of the hit position (assuming that light propagates at the same speed to both fiber ends) and thus no correction is required.

The fibre ends are coupled directly to the surface of SiPMs on both sides. For easy detector assembly and maintainability, the coupling will be done by using mechanical pressure (spring loading) of the fibres to the SiPM without the use of glue or optical grease. Due to space constraints, no extensive fan-out of fibres to the SiPM array channels is possible.

The Mu3e fibre detector uses the Hamamatsu S13552-HRQ SiPM arrays with a high quenching resistor (see figure 1.13). This sensor was developed for the LHCb experiment. Different than in LHCb, where the SiPMs are operated around −40 °C, the Mu3e sensors operate at room temperature but also in a much less intense radiation field. We are exploring the possibility to cool the SiPM arrays to 5 °C, the same temperature of the Mu3e cooling, in order to further reduce the dark count rate and limit the radiation damage effects.

Each channel of the multi-channel SiPM out of two dies each with 64 channel arranged in a one-dimensional array consists of 104 pixels with a size of 57.5 µm × 62.5 µm arranged in a 4 × 26 grid resulting in a channel area of 230 µm × 1625 µm. The pixels are separated by trenches of the fifth generation Hamamatsu low-crosstalk development (LCT5). The channels have a pitch of 250 µm, and a gap of 220 µm separates the two dies in the centre of the sensor. They share a common cathode. The overall current consumption of one array

[2]With contributions from quantum efficiency and geometrical fill factors.

is expected to be well below 1 mA. The sensors are delivered wire bonded to a PCB with solder pads on the backside and covered with a 105 µm thick epoxy resin. Figure 1.13 shows such an assembly. Table 1.2 summaries the most important features of this sensor.

Figure 1.14 shows the I-V curves for the SiPM array for each channel of the array. All breakdown voltages are comprised within ±0.25 V of the central value of 52.5 V for this device. The performance of the photo-detector can be further improved by adjusting individually the operational voltage for each channel of the array. This is possible thanks to the MuTRiG ASIC, which allows for the fine tuning of the bias voltage around a common value.

1.3 SciFi Readout Electronics

The Mu3e scintillating fibre detector requires the digitization of the Time of Arrival (ToA) at a single photon level where very little space is available. Furthermore, the readout electronics has to cope with up to 650 MHz signal from particle crossing the detector in combination with up to several 100 MHz DCR on a single photo-electron trigger level. Due to the space constraints, the usage of a mixed-mode ASIC is required. Although many state-of-the-art ASIC for digitization of SiPM signals exists, none can handle the required rates. MuTRiG was developed within the Mu3e collaboration based on STiC to fulfill the

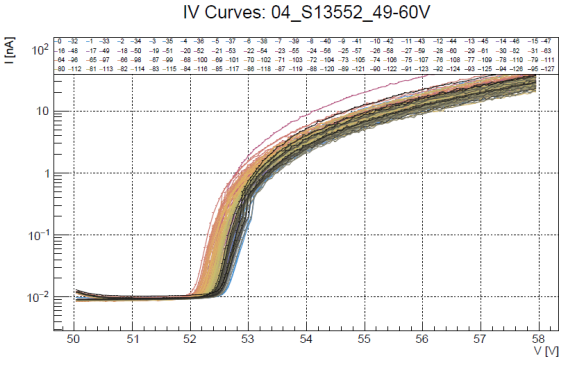

Figure 1.14: I-V curves for the SiPM array showing the breakdown voltage for each channel of the array. All breakdown voltages are comprised within ±0.25 V of the central value of 52.5 V.

detectors requirement (see chapter **??**); the tile sub-detector uses the same SiPM readout chip.

In contrast to the PET applications (usually LYSO crystals as scintillator) for which STiC was originally designed and the tile sub-detector where signals consist of ∼ 1000 photons, the fibre detector readout has to operate with very few photons. MuTRiG fulfills the fibre detector requirement in a special mode, where the event validation by a second threshold (*energy threshold*) is switched off, and the *energy*-time-stamp is reduced to a single flag.

For the readout of the 3000 channels of the fiber detector we plan to use the MuTRiG ASIC: a mixed signal Silicon Photomultiplier readout ASIC with high timing resolution and gigabit data link. The MuTRiG chip comprises 32 input fully differential channels with 50 ps TDC time binning. 4 chips are required for the readout of one SiPM array, and 96 for the full detector. The analog part is complemented by digital readout logic and a 1.28 Gb/s LVDS serial data link. When operated with the SiPM arrays two thresholds will be used: a low one for timing (a time stamp will be generated) and a high one for hit selection. Moreover, MuTRiG allows for the fine tuning of each SiPM bias voltage, which is required for the optimal operation of our SiPM arrays (see Figure 1.14).

The analogue signals from each SiPM array (128 channels) are digitized by one SciFi front end board. Each SiPM array is connected via a flex-print to a front end board hosting 4 MuTRiG chips. Due to the limited space the design of the front end board is very compact. The boards sit below the SciFi ribbons (see next section). In addition to the MuTRiG chips, the front board comprises the clock distribution, components for the control of the MuTRiG chips, power distribution, and temperature monitoring. Finally each front end board is connected to readout boards via a very thin set of twisted pair cables.

1.4 Performance

Scintillating fibre ribbon prototypes coupled to SiPM arrays of the latest version have been tested intensively in test beams at CERN PS (T9 beamline) and PSI (πM1 beamline), and with ^{90}Sr sources, as well. Data were recorded using a fast pre-amplifier and readout digitizing electronics based on the DRS4 ASIC. The recorded wave-

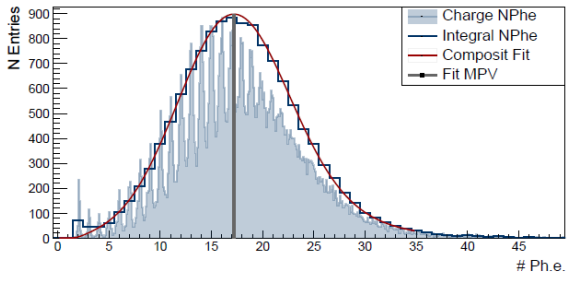

Figure 1.15: Cluster light yield of a three layered SCSF-78MJ fiber ribbon prepared with clear epoxy. The integral NPhe is obtained by integrating the charge in a region of ±0.5 ph.e. around each integer. A convolution of a Gaussian and Landau is used to fit the data and the most probable value (MPV) is marked with a line.

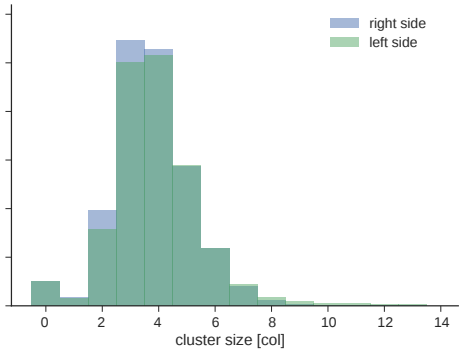

Figure 1.16: Cluster size of both sides of a 3 layer NOL-11 ribbon without any additional coating.

forms were then processed using timing algorithms close to the MuTRiG functioning (i.e. 0.5 ph.e. low threshold leading edge discriminator).

Figure 1.15 shows the light yield of a cluster for a 3-layered SCSF-78MJ fiber ribbon prepared with clear epoxy. A cluster consists of all consecutive columns with an amplitude larger than a specific threshold (0.5 ph.e.). The integral NPhe is obtained by integrating the charge in a region of ±0.5 ph.e. around each integer. A convolution of a Gaussian and Landau is used to fit the data. This information, however, will not be accessible in the experiment since the MuTRiG ASIC provides only the timing information and no charge information.

The cluster size distribution of a 3-layer NOL-11 ribbon without any additional coating is shown in figure 1.16. Typical cluster sizes are around 3.5

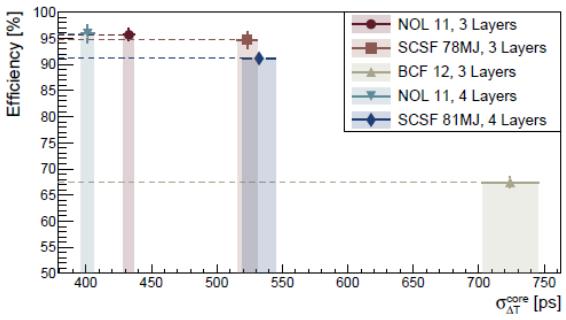

Figure 1.17: Detection efficiencies vs their respective time-difference resolutions for selected ribbons. The efficiency is estimated for an AND configuration (i.e. require hits at both ribbon ends) and the minimal cluster multiplicity of two neighbouring channels with an amplitude of at least 0.5 ph.e. Events are considered valid if they fall within the area of $\pm 3\sigma$ around the centroid of the time difference Gaussian fit. The efficiency estimates are conservative and represent a lower limit. No channel by channel time offset correction is applied in extracting the timing resolution. Note that the figure shows the time difference resolution. For the mean time the resolution is half the one reported in the figure.

for a threshold of 0.5 ph.e. The cluster size can be reduced by increasing the detection threshold to e.g. 1.5 ph.e. The difference of cluster sizes between both sides is caused by slightly different mappings of the ribbons to the SiPM arrays.

Figure 1.17 summarizes the detection efficiency versus timing resolution for selected fiber ribbons assembled using different scintillating fibers. The resolution of the time difference from the two ribbon sides $\sigma(t_{\text{left}} - t_{\text{right}})$, obtained with a leading edge algorithm, corresponds to twice the intrinsic resolution σ_{ribbon} (mean time).

Similar timing performances have been obtained also with the MuTRiG ASIC. Figure 1.18 shows an example time difference distribution for clusters with a minimum size of 2, obtained with a sensor biased at 58.2 V. The resolution of the time difference from the two ribbon sides $\sigma(t_{\text{cl, left}} - t_{\text{cl, right}})$ correspond to twice the intrinsic fibre prototype resolution $\sigma_{\text{cl, ribbon}}$. It agrees very well with the time resolution extracted by the DRS4-based DAQ of the same ribbon. For example, the FWHM/2.35 obtained in the MuTRiG measurement of 366(13) ps lies very well inside the uncer-

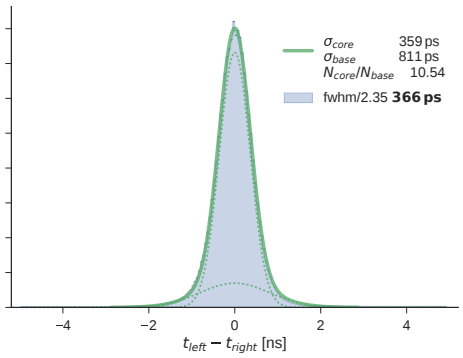

Figure 1.18: Time Resolution of a 4 layer SCSF-78MJ ribbon without additional TiO_2 in the glue extracted from clusters with at least 2 active columns. No channel by channel time offset correction is applied.

tainty of 361(23) ps obtained in the full waveform test beam analysis.

1.5 Fibre Mechanics

Three considerations determine the SciFi detector location. Firstly, no material should be placed outside of the fourth pixel layer where the main momentum measurement is performed. Secondly, it has to be in close vicinity to a pixel layer. The track finding algorithm considers scattering alone in this layers. And thirdly, the larger the radius is, the smaller the sub-detectors occupancy and resulting pile-up.

Figure 1.19 shows the overall design of the SciFi detector. The detector is composed of 12 SciFi ribbons, 300 mm long and 32.5 mm wide. The SciFi ribbons are staggered longitudinally (around 10 mm) in order to reduce dead spaces between

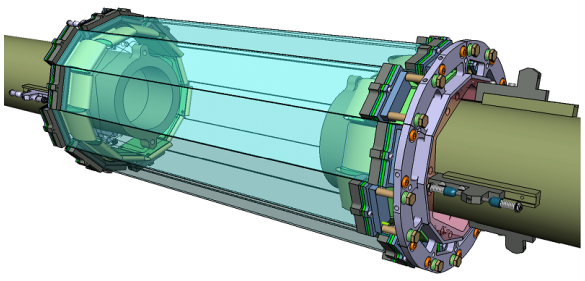

Figure 1.19: Overall view of the fibre detetor.

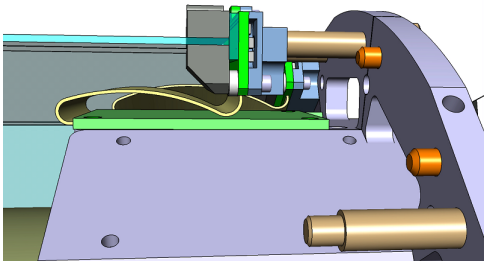

Figure 1.20: Detailed side view of the fibre detector, showing the fibre ribbon coupled to the SiPM array and the SciFi front end board connected to the array via a flex-print. The front end board is fixed on a cooling plate.

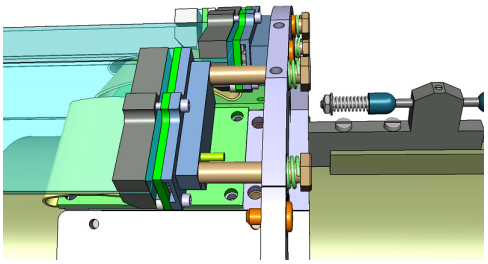

Figure 1.21: Detailed top view of the fibre detector at one fiber end.

the ribbons. The ribbons are spring loaded on one side (6 ribbons on one side and the other 6 on the other side) to compensate for the thermal expansion and to provide sufficient tension to avoid sagging. For forces larger than 0.3 N a sag below a mm is observed what is believed to be sufficient for this detector.

The SciFi ribbons are coupled to the SiPM arrays by simple mechanical pressure (no grease or other optical interface) and the arrays are connected to front end boards via a flex-print. The front end boards are fixed to cooling plates to dissipate the heat produced by the MuTRiG ASICS (around 1 W of heat power is generated by one ASIC, therefore 50 W have to be dissipated on each side of the SciFi detector) Figures 1.20 and 1.20 show a detailed side and top view of this structure. To facilitate the installation two SciFi ribbons are attached to the same fibre support structure to form one module. The two ribbons are offset along the beam direction by 10 mm to accommodate the photo-sensors.

1.5.1 The Electrical Connection

The electrical connection between the sensors and the readout electronics is realized through the flex-print cables, which end at the bottom of the module support structure. First the 128 channel SiPM arrays are soldered to a support PCB with embedded flex-prints, then the circuit continues to a second PCB hosting the MuTRiG ASICs. The flexibility is required to compensate for the distance difference caused by the spring loading. Furthermore, the SciFi front end boards are thermally connected to the cooling plates. This construction is repeated on both ribbons ends and for all ribbons.

1.5.2 Cooling Concept

The cooling of the SciFi detector splits into two parts. Firstly, the system has to discharge around 50 W per side dissipated by the readout ASICs and LDOs. This is realised directly through the liquid-cooled plates below the SciFi front end boards, which are connected to the cooling system of the Mu3e apparatus. Secondly, the temperature of the SiPM sensors is required to be stabilized, and possibly cooled down to the lowest possible temperature (4° C is the temperature of the liquid coolant). This will be implemented by adding an additional thermal contact between the SiPM PCB and the cooling plates.

Bibliography

[1] Kuraray, *SCINTILLATION MATERIALS*, 2014.

[2] Saint-Gobain Crystals, *Scintillation Products*, 2014.

[3] Giada Rutar, *In Search of Charged Lepton Flavor Violating Decays at PSI*, PhD thesis, ETH Zurich, 2017.

[4] Antoaneta Damyanova, *Characterization of the Mu3e Scintillating Fibre DetectorNOT YET FINAL*, PhD thesis, University of Geneva, in preparation.

[5] Simon Corrodi, *Towards the Mu3e Scintillating Fibre Detector*, PhD thesis, ETH Zurich, 2018, in preparation.

[6] Kuonena Axel, Haefelia Guido, Stramagliaa Maria, Elena and Olivier Girard, Characterisation of the Hamamatsu MPPC multichannel array for the LHCb SciFi Tracker v.11.2016, Technical report, EPFL, 2017.